communications earth & environment

ARTICLE

https://doi.org/10.1038/s43247-023-00727-3 OPEN

Human-induced changes in the global meridional overturning circulation are emerging from the Southern Ocean

Sang-Ki Lee[1✉], Rick Lumpkin[1], Fabian Gomez[2,1], Stephen Yeager[3], Hosmay Lopez[1], Filippos Takglis[4,1], Shenfu Dong[1], Wilton Aguiar[4,1], Dongmin Kim[4,1] & Molly Baringer[1]

In a warming climate, the Global Meridional Overturning Circulation (GMOC) is expected to change significantly with a risk of disrupting the global redistribution of ocean properties that sustains marine ecosystems, carbon cycle, and others. Here we make a novel attempt to utilize a diagnostic ocean & sea-ice model to estimate the GMOC and its interdecadal changes since the mid-1950s that are consistent with historical hydrographic observations. We find that significant changes in the GMOC have already occurred, most notably in the upper and lower overturning cells in the Southern Ocean. The former has expanded poleward and into denser water and strengthened by 3–4 *Sv* since the mid-1970s, while the latter has contracted and weakened by a similar rate during the same period. These changes are driven by the increasing Southern Hemisphere (SH) Ferrel cell and associated increases in the westerlies and the surface buoyancy loss over its sinking branch, and the increasing Antarctic meltwater discharge, in response to ozone depletion in the SH stratosphere and increasing atmospheric CO_2. A large-scale readjustment of the GMOC seems to be underway in the South Atlantic and Indo-Pacific Oceans since the mid-2000s in response to the Southern Ocean changes.

[1] NOAA Atlantic Oceanographic and Meteorological Laboratory, Miami, FL, USA. [2] Northern Gulf Institute, Mississippi State University, Mississippi State, MS, USA. [3] National Center for Atmospheric Research, Boulder, CO, USA. [4] Cooperative Institute for Marine and Atmospheric Studies, University of Miami, Miami, FL, USA. ✉email: Sang-Ki.Lee@noaa.gov

As the surface ocean warms and polar ice sheets melt due to increasing anthropogenic greenhouse gases in the atmosphere, near-surface stratification is increasing almost everywhere, including the major deep water formation regions in the high-latitude North Atlantic and around Antarctica[1]. Enhanced near-surface stratification inhibits the sinking of surface waters and thus may lead to a slowdown of the Global Meridional Overturning Circulation (GMOC, also referred to as the global thermohaline circulation[2] or the global conveyor belt[3] in the literature). A large-scale slowdown of the GMOC may, in turn, inhibit the redistribution of heat, salt, nutrients, and carbon between hemispheres and across ocean basins, and thus has important implications for marine ecosystems, carbon cycle, sea-level, climate, and extreme weather[4–10].

Numerous studies based on hydrographic observations have suggested that significant changes in the GMOC have already occurred during recent decades[11–24]. For example, the southward return flow of lower North Atlantic Deep Water (LNADW), the densest water mass in the high-latitude North Atlantic, decreased by about 30% during 2008–2016 compared to its value during 2004–2007[22]. Repeated hydrographic sections across the Southern Ocean showed that a significant contraction of the Antarctic Bottom Water (AABW) volume occurred between the 1980s and 2000s[15] with a freshening and warming of AABW observed throughout the Southern Ocean[11–14,16–21,24]. Hence, these and other direct observations collectively indicate a potential global reduction of deep and abyssal water formation, and thus a slowdown of the GMOC in recent decades.

These results are also consistent with projected changes in externally forced climate model simulations for the twenty-first century[25–31]. Despite some inter-model differences, externally forced climate models project a robust weakening of the Atlantic Meridional Overturning Circulation (AMOC), the Atlantic component of the GMOC, due to a surface warming and freshening of the Labrador, Irminger, and Greenland-Iceland-Norwegian Seas[26,27,31]. The climate models also project weakening AABW formation and its northward outflow and thus a slowdown of the lower overturning cell in the Southern Ocean[25,28–30]. On the other hand, the same models project a strengthening of the upper overturning cell in the Southern Ocean due to a strengthening of the Southern Hemisphere (SH) westerlies and associated surface buoyancy flux changes[25,28–30], driven by both ozone depletion in the SH stratosphere and increasing CO_2 in the atmosphere[32–36]. Although there are no direct observations supporting the strengthening upper overturning cell in the Southern Ocean, water mass age differences between the early 1990s and the late 2000s from measurements of chlorofluorocarbon-12 suggest a strengthening of the upper overturning cell[37]. Additionally, the majority of ocean & sea-ice models that have a proper representation of mesoscale eddy effects in the Southern Ocean (i.e., eddy compensation[38–41]) show a strengthening of the upper overturning cell since the 1970s when they are forced with historical surface flux fields, consistent with a strengthening of the SH westerlies and the associated surface buoyancy flux changes that occurred during the same period[42].

Thus, there is an overall agreement between observational studies and externally forced climate model projections that suggests a global reduction of deep and abyssal water formation and associated changes in the GMOC are already underway in response to increasing greenhouse gases and SH stratospheric ozone depletion. However, the observational records are generally too short and sparse to determine whether the observed trends are externally forced or due to natural low-frequency variability[43]. Additionally, the current state-of-the-art climate and ocean models have difficulties in reproducing the mean state of the GMOC[42,44]. These limitations underscore the need to reproduce the GMOC and its changes consistent with long-term averaged historical global hydrographic observations. Encouraged by success in reproducing directly-observed GMOC transport values in multiple transects as reported in two recent studies[44,45], here we use a diagnostic ocean & sea-ice model constrained by global hydrographic observations in an attempt to estimate the GMOC and its interdecadal changes since the mid-20th century. Specifically, we carried out a series of diagnostic ocean & sea-ice model simulations with the model temperature and salinity restored toward long-term averaged global hydrographic observations for each decade between 1955 and 2017 following the methodology presented in Lee et al.[44]. and other studies[45,46] ("Methods").

Results

The GMOC in density coordinates. Figure 1a, e–g and Fig. 2a, e–g show the GMOC transport streamfunction (contours) and its interdecadal changes (color shades) in density coordinates during 2005–2017, 1995–2004, 1985–1994 and 1975–1984 compared to the reference period of 1955-1974 in the Southern and Indo-Pacific Oceans, and the Atlantic Ocean, respectively. Figures 1b–d and 2b–d show the vertical profiles of overturning streamfunction at selected latitudes in the Southern and Indo-Pacific Oceans (65°S, 43°S and 30°S) and the Atlantic Ocean (30°S, 26.5°N, and 55°N), respectively. The differences in GMOC transport values between 2005–2017 and 1955–1975 for various water masses are also shown at these latitudes. Red colored values are for the increased transport values, and blue colored are for the decreased transport values.

The GMOC transport streamfunction (ψ) in density coordinates can be defined as follows

$$\mathrm{GMOC}(t,y,\sigma_2) = \psi(t,y,\sigma_2) = \int_{z(\sigma_b)}^{z(\sigma_t)} \int_{x_e}^{x_w} v(t,x,y,\sigma_2)\mathrm{d}x\mathrm{d}z \quad (1)$$

where t is time, z is depth, y is latitude, x is longitude, σ_2 is potential density referenced to 2000 m, and v is the meridional velocity. The integral is carried out from the western end (x_w) to the eastern end (x_e), and from the depth of the surface density ($z(\sigma_{2t})$) to the depth of the bottom density ($z(\sigma_{2b})$). See Supplementary Figure 1 for a schematic of the GMOC and the list of water masses referenced in this study[44,47,48].

The Southern and Indo-Pacific Oceans. As summarized in Fig. 1, the data-constrained model simulations show a robust strengthening and poleward-downward (in density space) expansion of the upper overturning cell in the Southern Ocean since the mid-1970s. For convenience, Circumpolar Deep Water (CDW) is divided into Upper (UCDW) and Lower Circumpolar Deep Water (LCDW) in such a way that UCDW feeds the upper overturning cell while LCDW eventually feeds the lower overturning cell in the Southern Ocean. At the core latitude of the upper overturning cell (43°S), the poleward transport of UCDW is increased by 3.5 *Sv* in 2005–2017 compared to its value in the reference period of 1955–1974 (a 56% increase from the total transport of 6.3 *Sv*, Fig. 1c). Note that the lower boundary of UCDW at which the transport streamfunction (ψ) becomes zero (by definition) is displaced downward into denser water. This is compensated by an increase in the equatorward transport of surface and intermediate waters (SFCW and IW by 3.5 *Sv*, $\sigma_2 < 36.70$). The formation rate of Antarctic Intermediate Water (AAIW) and Sub-Antarctic Mode Water (SAMW), inferred from the overturning streamfunction immediately north of on average 43°S, is increased by up to 3 *Sv* (Fig. 1c). This is consistent with the observed decrease in the age of SAMW from the early 1990s

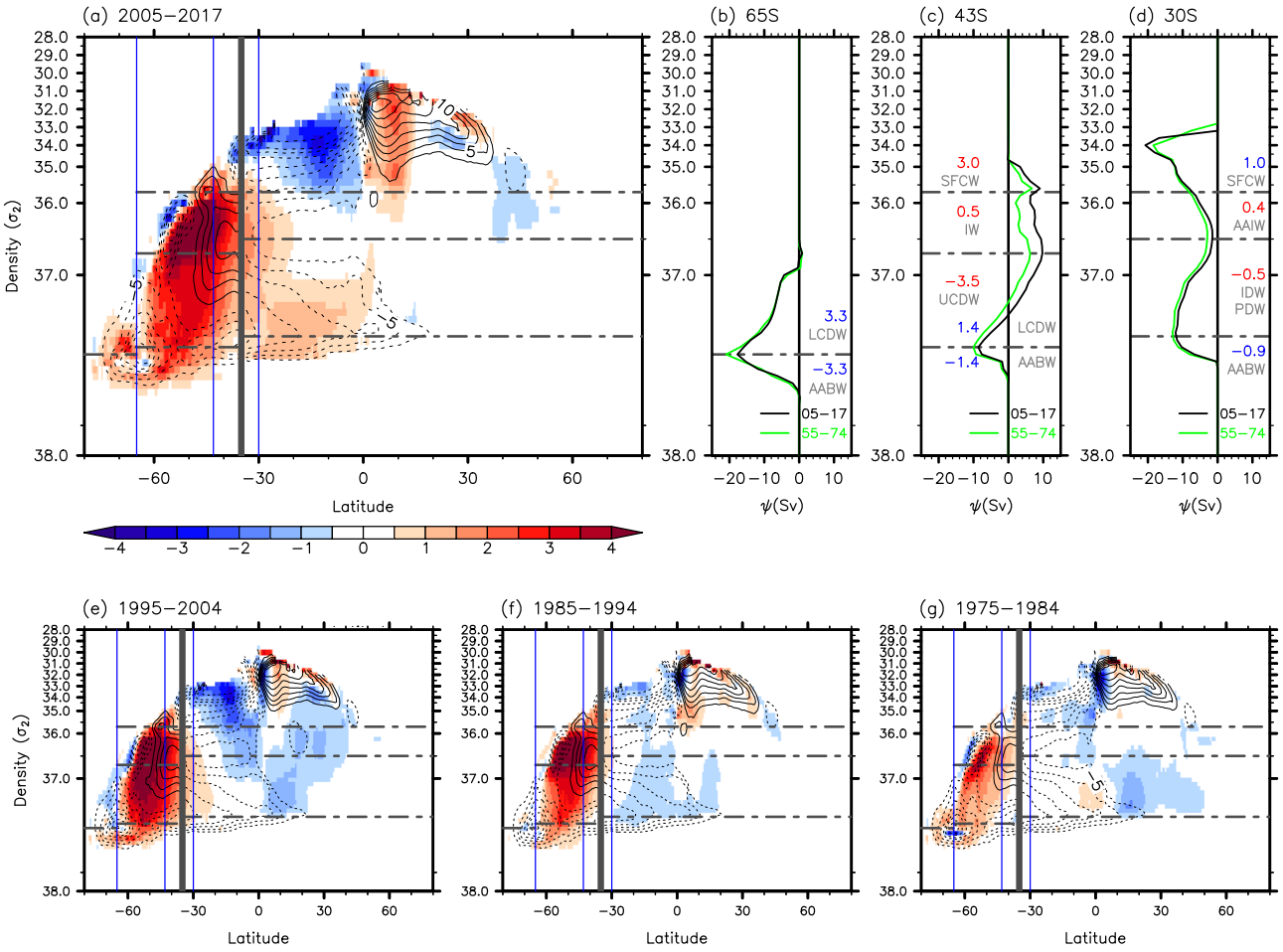

Fig. 1 The GMOC and its interdecadal changes in the Indo-Pacific and Southern Oceans. The GMOC volume transport streamfunction (contours) in the Southern Ocean (south of 35°S) and the Indo-Pacific Ocean (north of 35°S) and its changes (shades) during **a** 2005–2007, **e** 1995–2004, **f** 1985–1994, and **g** 1975–1984 in reference to the base period of 1955–1974. The GMOC volume transport streamfunction at **b** 65°S and **c** 43°S in the Southern Ocean, and at **d** 30°S in the Indo-Pacific Ocean during 2005–2007 (black lines) and 1955–1974 (green lines). The vertical axis is potential density in reference to 2000 m (σ_2 units). The differences in GMOC volume transport values between 2005–2017 and 1955–1975 for SFCW, AAIW, IW, UCDW, LCDW, IDW & PDW and AABW are shown at **b** 65°S, **c** 43°S, and **d** 30°S. Red colored values are for the increased transport values, and blue colored are for the decreased volume transport values. Black-dotted lines indicate the density ranges of water masses. Volume transports are in *Sv* units.

to the late 2000s detected through measurements of chlorofluorocarbon-12[37]. The enhanced formation of AAIW and SAMW provides the important pulling mechanism required to sustain the strengthened upper overturning cell. This point is discussed in more detail in later sections. Hereafter, if not specified, AAIW and SAMW are referred to as AAIW for simplicity because they have almost identical T-S properties in the southeast Pacific and southwest Atlantic regions where AAIW mainly forms[49,50].

The persistent strengthening and poleward-downward (in density space) expansion of the upper overturning cell is accompanied by a weakening and contraction of the lower overturning cell, consistent with a decrease in the AABW volume observed throughout the Southern Ocean since the 1980s[15]. Specifically, at the core latitude of the lower overturning cell (65°S), the outflow of AABW is decreased by 3.3 *Sv* in 2005–2017 compared to its value in 1955–1974 (a 16% decrease from the total transport of 21.0 *Sv*, Fig. 1b). This is compensated by a reduced poleward transport of LCDW. The reduced outflow of AABW is also evident at 43°S (by 1.4 *Sv* in 2005–2017 compared to its value in 1955–1974, a 14% decrease from the total northward transport of 10.0 *Sv*), which is compensated by a reduced poleward transport of LCDW (Fig. 1c). At this latitude, the upper boundary of LCDW, at which the transport streamfunction (ψ) becomes zero, is displaced downward into denser water.

It is interesting to note that there is a near-cancelation between the increase in the poleward UCDW transport (by 3.5 *Sv* at 43°S) and the decrease in the poleward LCDW transport (by 3.3 *Sv* at 65°S) (Fig. 1b, c). This indicates that the net upward transport of CDW averaged between 43°S and 65°S remains almost the same in 2005–2007 compared to the reference period in 1955–1974. The near-cancelation of the upward CDW transport change is well reflected in the poleward and downward (in density space) expansion of the upper overturning cell and the contraction of the lower overturning cell between 43°S and 65°S. In other words, the increase in water mass supply to the upper overturning cell and the decrease in water mass supply to the lower overturning cell are largely achieved through a realignment of the boundary between the upper and lower overturning cells within the Southern Ocean.

In response to the altered overturning cells in the Southern Ocean, a large-scale readjustment of the GMOC is slowly underway in the Indo-Pacific Ocean during the most recent decade (Fig. 1a). Specifically, the import of AABW across 30°S ($\sigma_2 > 37.17$) into the Indo-Pacific Ocean is reduced by about

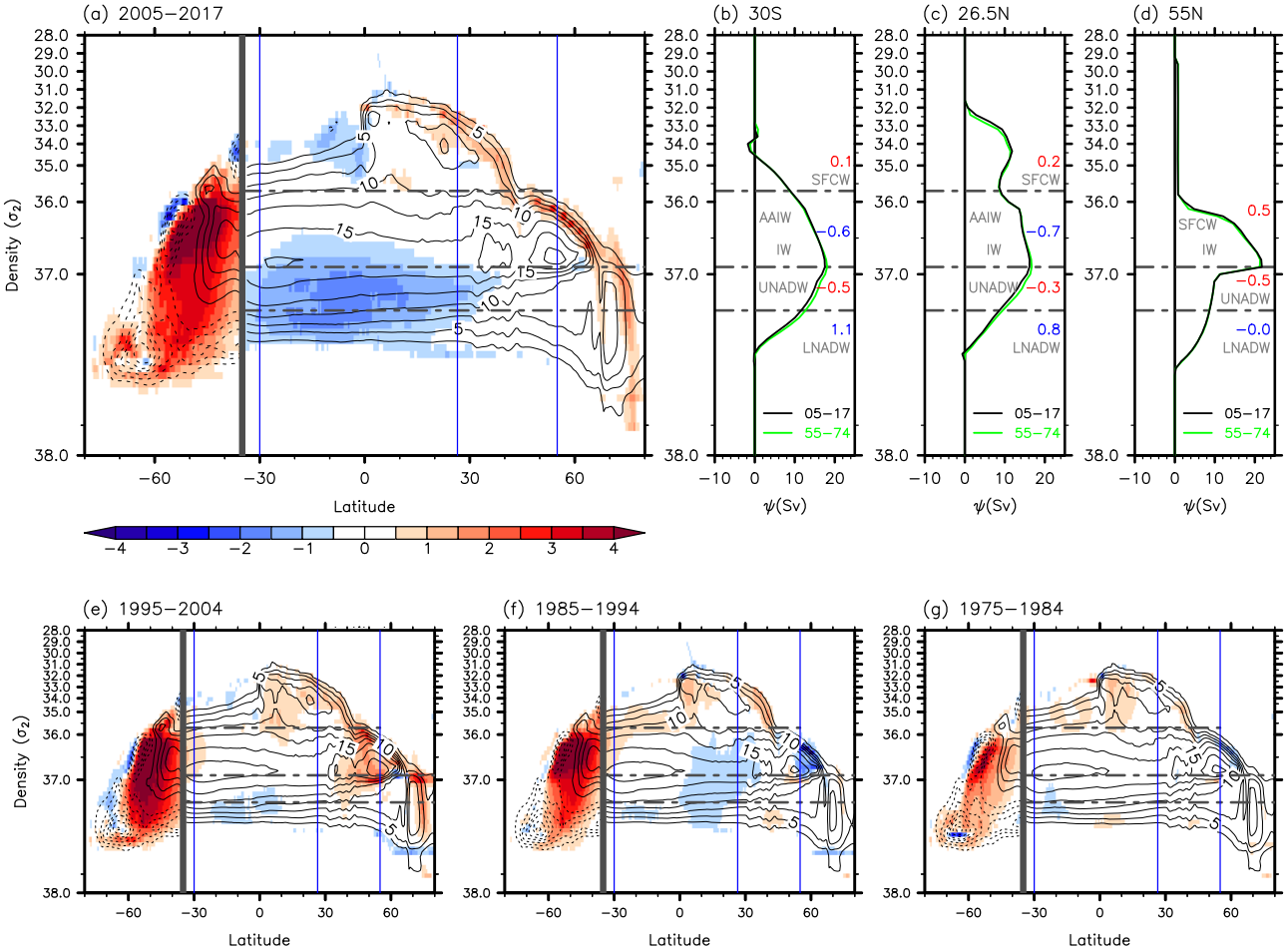

Fig. 2 The GMOC and its interdecadal changes in the Atlantic and Southern Oceans. The GMOC volume transport streamfunction (contours) in the Southern Ocean (south of 35°S) and the Atlantic Ocean (north of 35°S) and its changes (shades) during **a** 2005–2007, **e** 1995–2004, **f** 1985–1994, and **g** 1975–1984 in reference to the base period of 1955–1974. The AMOC volume transport streamfunction at **b** 30°S, **c** 26.5°N and **d** 55°N during 2005–2007 (black lines) and 1955–1974 (green lines). The vertical axis is potential density in reference to 2000 m (σ_2 units). The differences in AMOC volume transport values between 2005–2017 and 1955–1975 for SFCW, AAIW, IW, UNADW and LNADW are shown at **b** 30°S, **c** 26.5°N, and **d** 55°N. Red colored are for the increased transport values, and blue colored are for the decreased transport values. Black-dotted lines indicate the density ranges of water masses. Volume transports are in *Sv* units.

0.9 *Sv* during 2005–2017 compared to its value during 1955–1974 (a 7% decrease from the total transport of 12.9 *Sv*, Fig. 1d). Across the same latitude, the poleward export of Indian Deep Water & Pacific Deep Water (IDW & PDW, $36.50 > \sigma_2 > 37.17$), which is a source of UCDW in the Southern Ocean, increases slightly by about 0.5 *Sv* (a 5% increase from the total transport of 10.0 *Sv*), and thus provides a portion of the extra water mass supply for the enhanced upper overturning cell in the Southern Ocean. The increased poleward export of IDW & PDW across 30°S is in turn largely compensated by an increase in the import of AAIW ($35.70 > \sigma_2 > 36.50$) from the Southern Ocean by about 0.4 *Sv* (a 9% increase from the total transport of 4.3 *Sv*). The net poleward transport of the surface water (SFCW, $35.70 < \sigma_2$) across 30°S is reduced by about 1.0 *Sv* (a 14% decrease from the total transport of 7.2 *Sv*) closing the mass transport balance at that latitude. See Supplementary Figure 2 for more details of the results for the 1975–1984, 1985–1994 and 1995–2004 periods.

The Atlantic Ocean. As shown in Fig. 2a, the largest interdecadal signal in the Atlantic Ocean is the appearance of negative streamfunction anomalies between 30°S and 26.5°N in 2005–2017, centered around $\sigma_2 = 37.10$ between LNADW ($\sigma_2 > 37.10$) and Upper North Atlantic Deep Water (UNADW, $36.90 > \sigma_2 > 37.10$). Consequently, the southward LNADW transport is reduced by 1.1 *Sv* at 30°S (a 9% reduction from the total transport of 12.7 *Sv*), and by 0.8 *Sv* at 26.5°N (an 8% reduction from the total of 9.5 *Sv*), whereas the southward UNADW transport is slightly increased by 0.5 *Sv* at 30°S (a 9% increase from the total transport of 5.4 *Sv*), and by 0.3 *Sv* at 26.5°N (a 4% increase from the total of 7.2 *Sv*) (Fig. 2b, c). This suggests a shoaling of the AMOC south of 26.5°N. Additionally, since the reduction of the southward LNADW transport is greater than the increase in the southward UNADW transport, the net southward return flow is decreased by 0.5–0.6 *Sv* at 30°S and 26.5°N. To compensate for the net decrease in the southward return flow, the northward transport of IW ($36.50 > \sigma_2 > 36.90$) is decreased by about 0.6–0.7 *Sv* with little change in the northward transport of SFCW ($35.70 > \sigma_2$) or AAIW ($35.70 > \sigma_2 > 36.50$) at 30°S and 26.5°N.

However, the AMOC at its core latitude (55°N) is slightly increased (Fig. 2d) and thus is disconnected from the reduced AMOC south of 26.5°N. At this latitude, the AMOC transport displays large-amplitude interdecadal variability (Fig. 3b). In particular, the AMOC transport at 55°N is increased by 2.1 *Sv* in 1995–2004 and decreased by 0.9 *Sv* in 1985–1994 compared to its value in 1955–1974 (Supplementary Fig. 3d, h). According to

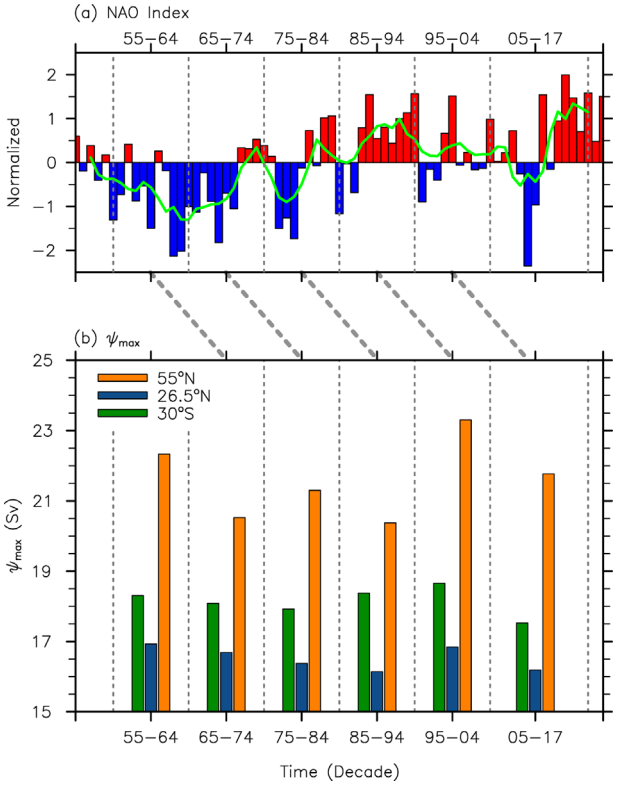

Fig. 3 Winter NAO index and AMOC. a Normalized winter (December-February) NAO index from 1950 to 2020. **b** The maximum AMOC volume transport at 30°S (green color bars), 26.5°N (blue color bars), and 55°N (dark orange color bars) in 1955–64, 1965–1974, 1975–1984, 1985–1994, 1995–2004, and 2005–2017. Green line in (**a**) indicates 5-year running averaged winter NAO index. Thin dashed lines in (**a**) and (**b**) mark the start and end of the decadal periods. Thick dashed lines between (**a**) and (**b**) link the NAO index with the maximum AMOC with 10-year time delay. Volume transports are in *Sv* units.

ocean & sea-ice models forced with historical surface flux fields, the North Atlantic Oscillation (NAO) is the main driver of AMOC variability at interannual to interdecadal time scales[51–53]. However, due to a baroclinic adjustment time of the subpolar North Atlantic Ocean circulation, it takes 3–15 years for the AMOC to respond to the NAO-induced surface buoyancy forcing and associated deep water formation[51,54,55].

This suggests that the large increase in the AMOC at 55°N in 1995–2004 is a delayed response to a strong phase of the NAO in 1985–1994, which is closely tied to the deepest and densest Labrador Sea Water formed during that period[56] (Fig. 3). Similarly, it is likely that the relatively weak AMOC transport at 55°N during the decades prior to and after 1995–2004 are due to the relatively weak NAO phases and associated reductions in Labrador Sea Water formation prior to 1985–1994 and after 1995–2004[56]. These results suggest that the AMOC changes at 55°N during the past several decades are not externally forced by increasing greenhouse gases but largely modulated by long-term natural climate variability associated with the NAO[52,53]. Indeed, similar interdecadal AMOC variations are also evident at 26.5°N and 30°S (Fig. 3b). This conclusion is also consistent with several recent studies based on various proxies, historical transects and ocean reanalyses[43,57–59], including two recent AMOC reconstructions for the past 30 years[58,59]. Therefore, it is likely that the previously reported weakening of the AMOC at 26.5°N during 2008–2016 compared to its value during 2004–2007[22] is due to long-term natural climate variability associated with the NAO.

However, some proxy-based studies suggested a long-term reduction in the AMOC since the earlier twentieth century[60,61]. What this suggests is that a potential long-term weakening of the AMOC linked to key drivers or proxies[53,62–65] may be embedded in the NAO-dominated AMOC variability during the past several decades. Such drivers (or proxies) include a gradual freshening of the Labrador Sea linked to increasing Greenland meltwater discharge[62], a reduction of the ocean-to-air turbulent flux over the Greenland and Iceland Seas due to rapidly rising air temperatures[63], a potential impact of retreating sea-ice cover along the regional boundary currents[64], and a spreading of Arctic surface waters into the North Atlantic through Fram and David Straits[65]. However, none of these potential drivers from the high-latitude North Atlantic or the Arctic region can explain why the southward LNADW transport between 30°S and 26.5°N is at its minimum value in 2005–2017 (Fig. 2 and Supplementary Fig. 3), while the AMOC at 55°N is still stronger in 2005–2017 compared to its values during 1965–1974, 1975–1984 and 1985–1994 periods (Fig. 3b). An alternative explanation is that the AMOC changes south of 26.5°N during 2005–2017 in reference to 1955–1974 are driven from the Southern Ocean. Specifically, given that LNADW is the primary source of LCDW that feeds the lower overturning cell in the Southern Ocean, the reduced southward transport of LNADW is consistent with the weakened and contracted lower overturning cell in the Southern Ocean. Similarly, the increased southward return flow of UNADW is in line with the increased poleward transport of UCDW and the associated strengthening of the upper overturning cell in the Southern Ocean. This hypothesis supports the notion that a large-scale readjustment of the AMOC is gradually underway during the most recent decade (2005–2017) in response to the altered overturning cells in the Southern Ocean.

Anthropogenic drivers for the Southern Ocean. The strengthening and poleward-downward expansion of the upper overturning cell south of 35°S is consistent with the strengthening SH westerlies and the associated increase in Ekman transport since the mid-1970s (Fig. 4 in the left panels), which is primarily caused by ozone depletion in the SH stratosphere and increasing CO_2 in the atmosphere[32–36]. However, the increased Ekman transport alone cannot sustain the strengthened upper overturning cell. There must be additional surface buoyancy loss and associated water mass transformation[66,67]. Otherwise, the increased Ekman transport is almost completely compensated by eddy-induced poleward transport in the Southern Ocean (i.e., eddy compensation[38–41]). The required additional pulling of the upper overturning cell is mainly provided by reduced precipitation minus evaporation (i.e., $\Delta(P-E)<0$)[68,69] and associated surface buoyancy loss across the sub-Antarctic region approximately between 50°S and 35°S (Fig. 4 in the left panels). More specifically, the net buoyancy loss in the latitude band of approximately 45°S − 35°S is largely accomplished by a decrease in precipitation, and an increase in evaporation and associated latent cooling (Fig. 5b, c). These buoyancy loss terms overcompensate the buoyancy gain associated with reduced sensible heat flux and increased longwave radiation.

The meridional $\Delta(P-E)$ pattern poleward of 35°S, which is also a robust feature during the positive phase of the Southern Annular Mode[68–72], is mainly driven by SH stratospheric ozone loss (and by increasing CO_2 in the atmosphere to a lesser degree)[68,69]. More specifically, the increased P − E between the Antarctic coast and roughly 50°S is due to increased storm activity associated with the increased SH westerlies, whereas the decreased P − E across the sub-Antarctic region approximately between 50°S and 35°S is linked to an increase in the SH Ferrel

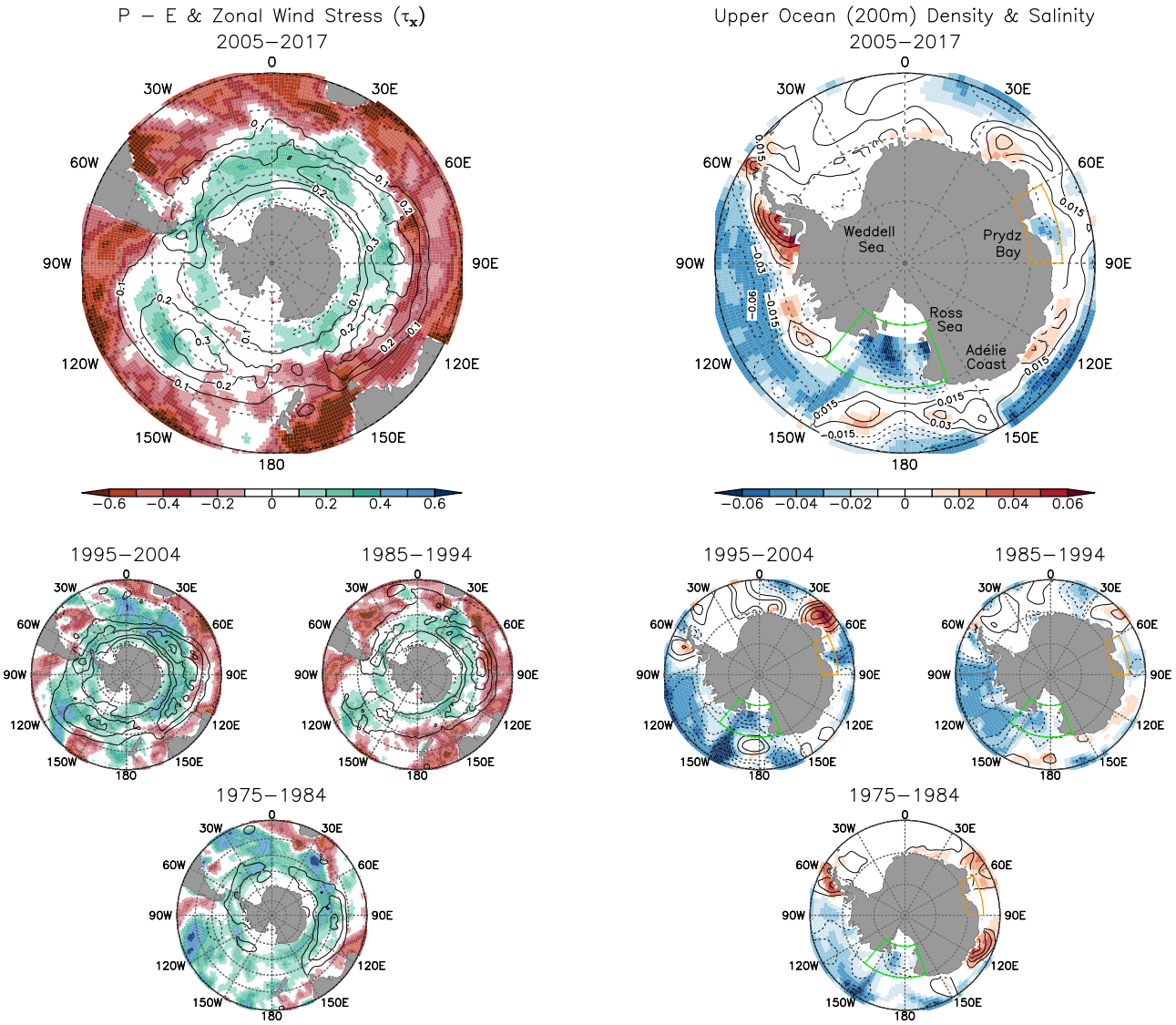

Fig. 4 Changes in surface forcing and upper ocean properties. Changes in (left panels) surface zonal wind stress (contours) and precipitation minus evaporation (P − E, shades) between 90°S and 30°S, and (right panels) upper 200 m density (shades) and salinity (contours) between 90°S and 60°S during 2005–2017, 1995–2004, 1985–1994 and 1975–1984 from the base period of 1955–1974. The units are dyne cm^{-2}, mm s^{-1}, σ_2, and PSU for wind stress, P − E, density, and salinity, respectively. Green boxes in the right panels indicate the Ross Sea region. Orange boxes in the right panels indicate the Prydz Bay area.

cell (Fig. 5) and the associated increase in atmospheric subsidence and poleward moisture transport (and thus moisture divergence and drying) in that latitude band[68–70,72]. The resulting net surface buoyancy loss between approximately 45°S and 35°S increases the rate of AAIW formation north of (on average) 43°S and thus explains up to 3 *Sv* of the total 3.5 *Sv* increase in the upper overturning cell (Fig. 1c).

It should be noted that the SH Ferrel cell is not only linked to P − E, but also to the SH westerlies via its modulation of the low sea-level pressure over the rising branch (65°S − 50°S), the high sea-level pressure over the sinking branch (45°S − 35°S) and the associated meridional sea-level pressure gradient. Therefore, the robust increase in the SH Ferrel cell since the mid-1970s is consistent with both the increasing SH westerlies and the increasing surface buoyancy loss over the sinking branch (Fig. 5). The links between SH stratospheric ozone loss, SH stratospheric cooling, and strengthening of the eddy-driven SH westerly jet and Ferrel cell are consistent with previous studies based on observations and model experiments[68,72].

According to some modeling studies, the enhanced SH westerlies increase the wind-driven upwelling of CDW to the surface enhancing both the upper and lower overturning cells[38–40,73]. This suggests that the weakening and contraction of the lower overturning cell are driven by some other processes. It is possible that the net buoyancy gains south of 45°S (Fig. 5b, c) contribute to the weakening and contraction of the lower overturning cell[28]. However, it should be noted that the lower overturning cell in the Southern Ocean is primarily driven by sinking of dense Antarctic shelf waters[66]. Figure 4 in the right panels indicates a persistent freshening of the surface water around the Ross Sea and associated reduction of the surface density (also near the Prydz Bay to a lesser degree) since the mid-1970s. This is well supported by earlier observational studies[74–76]. According to these studies, the enhanced melting of Antarctic ice shelves due to increasing CO_2 in the atmosphere increases the Antarctic meltwater discharge into the Amundsen-Bellingshausen Seas. The downstream (westward) transport of the extra freshwater into the Ross Sea via the Antarctic coastal current is directly

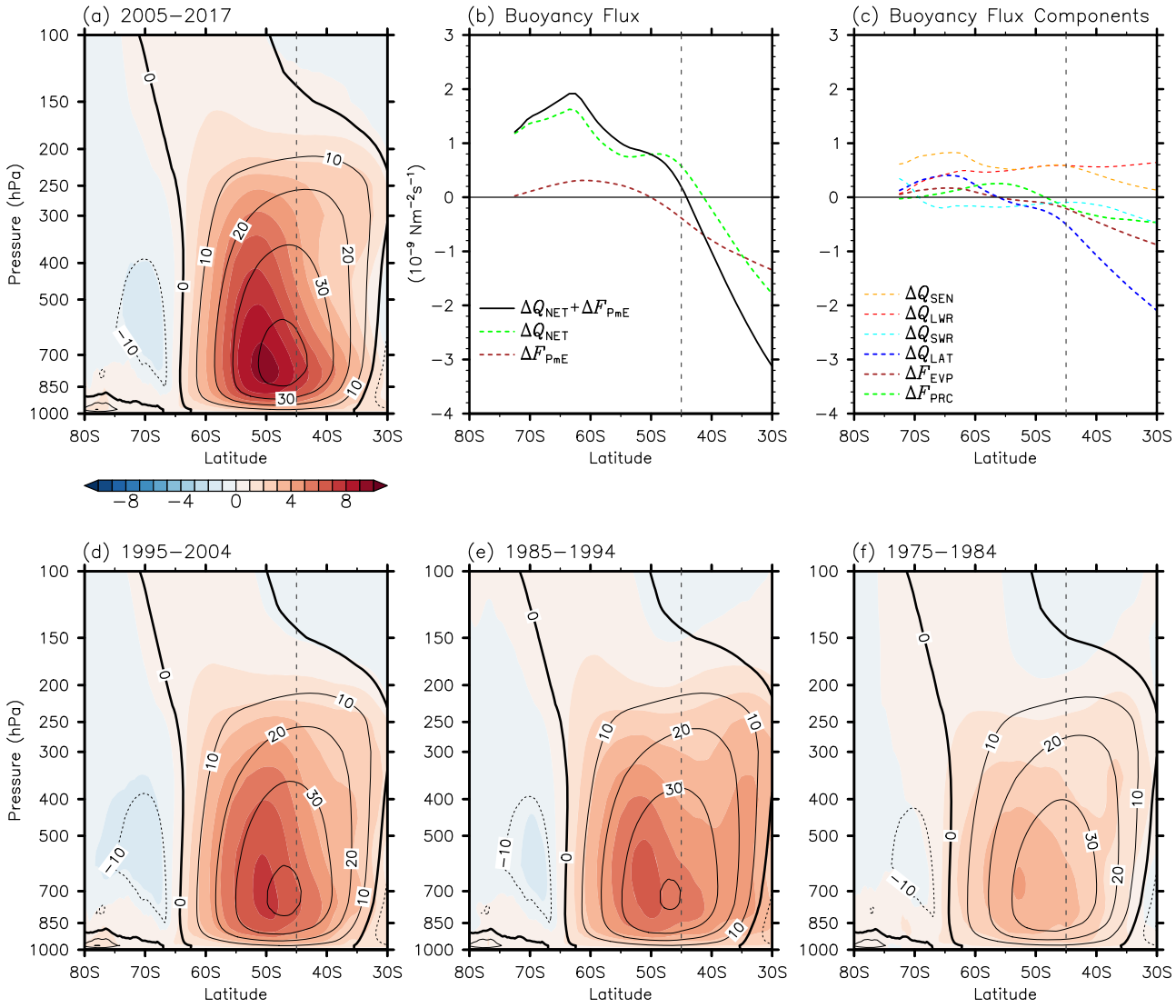

Fig. 5 SH Polar and Ferrel Cells and surface buoyancy flux. Mass transport streamfunction (10^9 kg s^{-1}) for the SH Polar and Ferrel cells (contours) and its interdecadal changes (shades) during **a** 2005–2017, **d** 1995–2004, **e** 1985–1994 and **f** 1975–1984 from the base period of 1955–1974, derived from the ERA5. Zonally averaged changes in (**b**) net buoyancy flux ($\Delta Q_{NET} + \Delta F_{PmE}$) and its associated heat and freshwater flux, and **c** heat and freshwater flux components in 2005–2017 in comparison to the reference period of 1955–1974. ΔQ_{NET}, ΔQ_{SEN}, ΔQ_{LWR}, ΔQ_{SWR}, ΔQ_{LAT}, ΔF_{PmE}, ΔF_{PRC}, and ΔF_{EVP} in (**b**) and (**c**) indicate the changes in net surface heat flux, sensible heat flux, longwave radiation, shortwave radiation, latent heat flux, net freshwater flux, precipitation and evaporation, respectively. All values in (**b**) and (**c**) are smoothed, and converted into buoyancy flux unit (10^{-9} Nm^{-2} s^{-1}) using a simplified linear equation and assuming that the thermal and saline expansion coefficients are constant. A positive flux value in (**b**) and (**c**) indicates a buoyancy gain, while a negative a buoyancy loss. Gray-dotted vertical lines indicate 45°S.

responsible for the freshening of the Ross Sea shelf waters. The increased near-surface stratification (i.e., buoyancy gain), in turn, reduces deep water formation around the Ross ice shelf, and thus leads to a decrease in the supply of AABW[17]. It is worthwhile to point out that the enhancement in Antarctic meltwater discharge is not explicitly included in the data-constrained model simulations[44], but its impact on salinity and density is implicitly accounted for via the restoration of model salinity toward observations.

Sensitivity of the data-constrained diagnostic ocean & sea-ice model. The data-constrained modeling approach employed in this study estimates global ocean circulations that are consistent with the decadally averaged World Ocean Atlas 2018 climatology[77,78] using a diagnostic ocean & sea-ice model ("Methods"). As such, the data-constrained model is subject to its inherent uncertainties originating from both the ocean & sea-ice model and observational datasets used. Therefore, it is further tested here to what extent the results derived from the primary set of data-constrained model simulations are robust with respect to two key sources of uncertainty, namely hydrographic temperature and salinity data, and surface forcing fields ("Methods").

Although there are some differences, a very good agreement is found in the GMOC and its interdecadal changes between the two model experiments constrained by the decadally averaged WOA18 and EN4 climatology[79,80] (Supplementary Figs. 4 and 5). Similarly, the GMOC and its interdecadal changes since the mid-1950s are overall consistent between the two model experiments forced by the European Center for Medium-Range Weather Forecasts reanalysis-5 (ERA5)[81] and the Japanese 55-year reanalysis (JRA55)[82] (Supplementary Figs. 6 and 7). The primary set of data-constrained model simulations and the two additional sets of sensitivity simulations are further used to estimate the

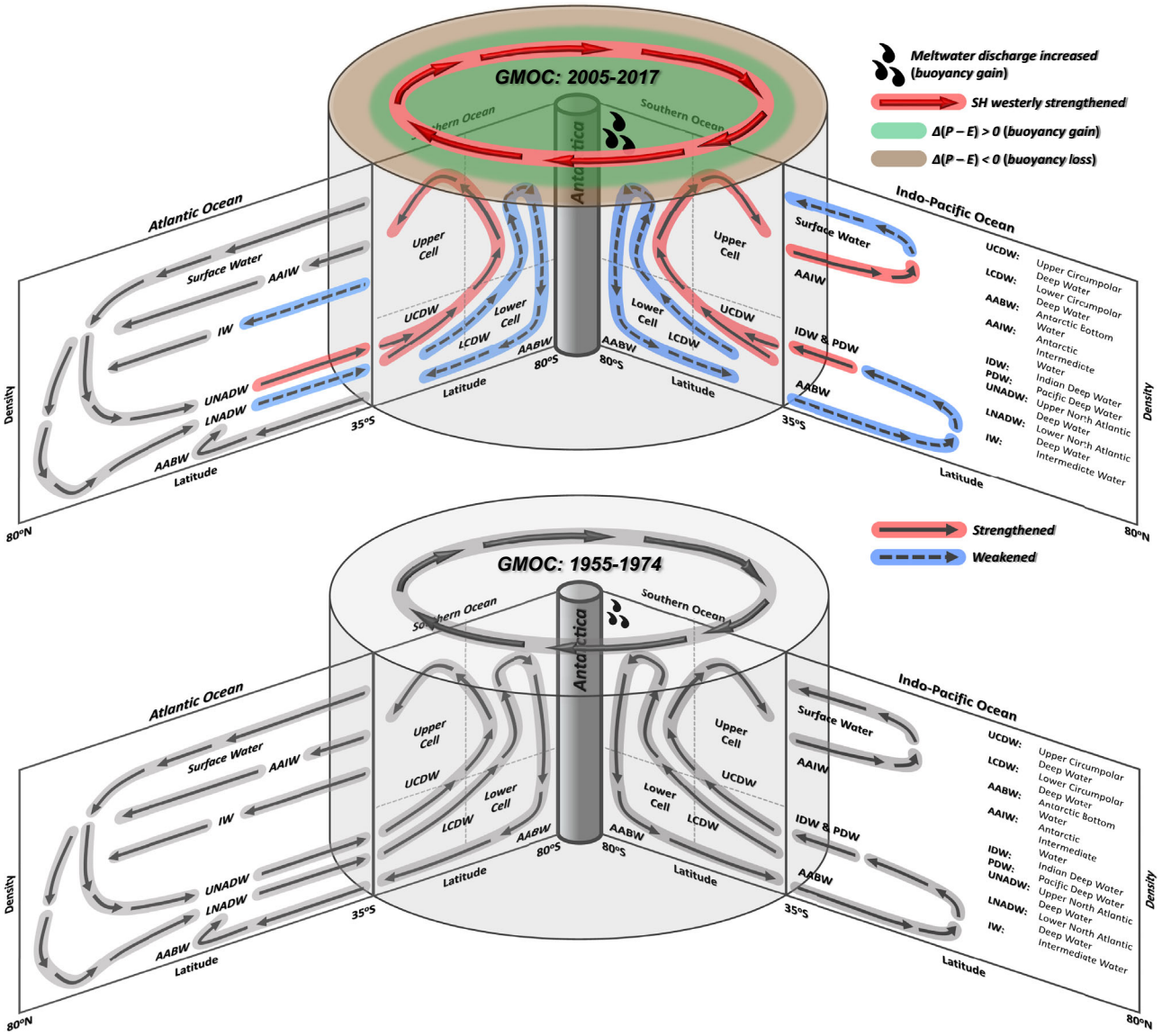

Fig. 6 Major changes in the GMOC and the drivers. A summary schematic of the GMOC in (upper panel) 2005–2017 and (lower panel) 1955–1974. Major changes in the GMOC and the associated increases in SH westerly and Antarctic meltwater discharge and P − E changes in 2005−2017 in reference to 1955–1974 are also indicated in the upper panel.

signal (mean) to noise ratio (standard deviation) of the differences in the GMOC transport values between 2005–2017 and 1955–1974 at selected latitudes (Supplementary Tables 1 and 2). For the key MOC transport components, the mean change is about 5–16 times larger than the standard deviation. For instance, in the Southern and Indo-Pacific Oceans, the outflow of AABW is reduced by $3.5 \pm 0.5\,Sv$ and $1.6 \pm 0.1\,Sv$ at 65°S, and 43°S, respectively, and by $1.0 \pm 0.2\,Sv$ at 30°S in the Indo-Pacific Ocean. The poleward transport of UCDW is increased by $3.1 \pm 0.3\,Sv$ at 43°S. In the Atlantic Ocean, the southward transport of LNADW is reduced by $0.9 \pm 0.2\,Sv$ at 30°S, while the southward transport of UNADW is increased by $0.5 \pm 0.1\,Sv$ at the same latitude. Therefore, although this is a primitive way to estimate the robustness of the results, the interdecadal changes in the GMOC reported in this study are overall consistent with respect to the hydrographic data and surface forcing fields used.

Discussion

In this study, we make a novel attempt to utilize a diagnostic ocean & sea-ice model to estimate the GMOC and its interdecadal changes in the Southern Ocean, the Indo-Pacific Ocean, and the Atlantic Ocean since the mid-1950s that are consistent with historical hydrographic observations. As summarized in Fig. 6, the upper overturning cell in the Southern Ocean has strengthened by 3–4 *Sv* (50–60% of the total) and expanded poleward and into denser water since the mid-1970s. This is driven by the strengthening SH Ferrel cell and the associated increases in the SH westerlies and the surface buoyancy loss over its sinking branch (45°S–35°S) that are mainly resulted from ozone depletion in the SH stratosphere (and increasing CO2 in the atmosphere to a lesser degree). The resulting push-pull by the enhanced Ekman transport and the increased AAIW formation north of (on average) 43°S drives and sustains the strengthening of the upper overturning cell. Conversely, the lower overturning cell in the Southern Ocean has weakened by 3–4 *Sv* (10–20% of the total) and contracted during the same period. This is due to the increased Antarctic meltwater discharge from the Amundsen-Bellingshausen Seas driven by increasing CO2 in the atmosphere, its downstream (i.e., westward) transport into the Ross Sea, and the associated reduction in AABW formation. The required

changes in the UCDW and LCDW supply to the upper and lower overturning cells are made possible primarily through a realignment of the boundary between the upper and lower overturning cells via diapycnal mixing and transformation within the Southern Ocean.

In response to the conspicuous changes in the upper and lower overturning cells in the Southern Ocean, a large-scale readjustment of the GMOC seems to be gradually underway in the South Atlantic and Indo-Pacific Oceans during the most recent decade (2005-2017). Notably, the outflow of AABW across 30°S into the Indo-Pacific Ocean is decreased by ~ 1 *Sv* (5−10% of the total), and the southward return flow of LNADW in the South Atlantic Ocean is also decreased by ~ 1 *Sv* (~10% reduction of the total) across 30°S. However, the AMOC changes in the high-latitude North Atlantic during the past several decades appear to be largely modulated by long-term natural climate variability associated with the NAO. Further analysis shows that these results derived from the primary set of data-constrained model simulations are overall robust with respect to two key sources of uncertainty, namely hydrographic temperature and salinity data, and surface forcing fields used.

There are some outstanding questions that require further clarification. Note that the large-scale changes in the upper and lower overturning cells are mostly confined within the Southern Ocean. Specifically, the supply chain of CDW from the South Atlantic Ocean (NADW) and the Indo-Pacific Ocean (IDW & PDW) across 30°S undergoes relatively small net poleward transport change in 2005–2017 (Figs. 1d and 2b) and even smaller changes in earlier periods (Supplementary Figs. 2 and 3). The implied imbalance in water mass supply at the core latitude of the upper cell (43°S) is resolved in part through a downward (in density space) expansion and contraction of the upper and lower cells, respectively; thus, an increasing portion of LNADW supplies the poleward UCDW transport, and a decreasing portion of LNADW supplies the poleward LCDW transport. However, it is somewhat unclear how to reconcile the increased AAIW formation north of (on average) 43°S (Fig. 1c). Since the net northward transport of AAIW is increased only slightly across 30°S (Figs. 1d and 2b), to close the mass balance between 43°S and 30°S, there must be local storage (i.e., adiabatic convergence) of AAIW with additional diapycnal mixing with IW and UCDW. This seems to be supported by a preferential ocean heat and freshwater storage over the latitude band where AAIW is subducted during the past several decades[83–85]. Further studies are required to better understand how and to what extent the shifting overturning circulation in the Southern Ocean permeates into the other ocean basins.

It is important to discuss some of the limitations in this study. According to Lumpkin and Speer[86], AABW spreads northward across 32°S into the South Atlantic at the rate of 5.6 ± 3.0 *Sv*, and is subsequently transformed via topography-linked mixing into southward-flowing LNADW. This is also supported by other observational studies[87]. However, the net northward transport of AABW in the South Atlantic nearly vanishes in the data-constrained model simulations. It appears that this drawback is linked to the vertical resolution of the ocean model used. Specifically, while a significant fraction (~50%) of AABW is found below about 2000 m in the Indo-Pacific Ocean, AABW in the South Atlantic is found mainly below 4000 m[87]. Since the model layer thickness is about 250 m below 4000 m, the northward penetration of AABW in the South Atlantic Ocean is not adequately represented in the ocean model used in this study.

Finally, there are other sources of uncertainty unexplored in this study. In particular, the ocean & sea-ice model used in this study is a non-eddy resolving resolution model and its treatment of some key processes is either parameterized or under-represented ("Methods"). As such, there is a need to use high-resolution (in both vertical and horizontal) models to fully resolve such processes, including eddy compensation in the Southern Ocean, AABW export into the South Atlantic Ocean, and eddy-rich fronts and boundary currents. Perhaps the most significant source of uncertainty in this study is the relatively poor spatial and temporal coverage of the hydrographic data before the beginning of the Argo period (the early-2000s). Although the data sparsity during the pre-Argo period is somewhat alleviated in this study by using decadally averaged hydrographic climatology, it is still worthwhile to carry out further studies to explore and quantify uncertainties of the data-constrained model results during the pre-Argo period. These and other shortcomings in our method call for a cautious interpretation of the results presented in this study. Nevertheless, this is the first study to report based on historical global hydrographic observations that a significant reshaping of the GMOC has already emerged from the Southern Ocean due to human activity, and is actively advancing into the other ocean basins.

Methods

Data and model used. In this study, we carried out a series of data-constrained diagnostic global ocean & sea-ice model simulations using the ocean & sea-ice model components of the National Center for Atmospheric Research (NCAR) Community Earth System Model version 1 (CESM1)[88] and the surface forcing fields derived from the European Center for Medium-Range Weather Forecasts reanalysis-5 (ERA5)[81]. Both the ocean and sea-ice model components have 320 grid points in longitude and 384 in latitude on a displaced pole grid, with a longitudinal resolution of about 1.0° and a variable latitudinal resolution of approximately 0.3° near the equator and about 1.0° elsewhere. The ocean model has 60 vertical levels.

It should be noted that CESM1 employs a variable coefficient in the eddy parameterization, which is often referred to as GM coefficient[89], as described in Danabasoglu and Marshall[90], instead of a constant value used in its earlier versions. This enables CESM1 to mimic eddy compensation by which changes in the wind-driven overturning circulation over the eddy saturated Southern Ocean are greatly reduced[40,41]. As such, CESM1 can reproduce the ocean response to increasing SH westerlies simulated by much higher-resolution ocean models that do not require an eddy parameterization[38].

Ocean model temperature & salinity restoring. In order to reproduce the GMOC and its interdecadal changes since the mid-1950s, the model temperature and salinity fields are relaxed to the decadally averaged World Ocean Atlas 2018 climatology (WOA18)[77,78] for each decade between 1955 and 2017 (i. e., 1955–1964, 1965–1974, 1975–1984, 1985–1994, 1995–2004, and 2005–2017). As such, the data-constrained model used in this study is in essence a diagnostic computation of ocean circulation consistent with historical temperature and salinity fields. Thus, it is not designed to explicitly simulate the full physical and transient processes, such as deep water convection, diapycnal mixing, surface water mass transformation, or propagation of specific Rossby waves that are known to drive the GMOC and its variability[91–94]. Instead, the data-constrained model relies predominantly on the geostrophic balance and mass continuity, constrained by long-term averaged hydrographic fields, to diagnose ocean circulation, water mass transformations, and thus the GMOC and its interdecadal variability.

The CESM1 ocean & sea-ice model was first spun up for 400 years with the model temperature and salinity fields relaxed to the long-term averaged WOA18 for the reference period of 1955–1974. In order to determine an optimal set of temperature and salinity relaxation coefficients for upper and deeper oceans, we carried out several experiments. In agreement with Lee et al.[44], when the relaxation coefficient below 200 m is increased beyond an e-folding time of ~3 years, the spatial pattern and strength of the GMOC become unrealistic. For the upper 200 m, the temperature and salinity relaxation coefficient can be increased up to an e-folding time of ~10 days while maintaining a realistic pattern of the GMOC. However, when the relaxation coefficient for the upper 200 m is decreased much below an e-folding time of ~1 year, interdecadal changes in the upper ocean temperature and salinity in the high-latitude North Atlantic significantly deviate from those of WOA18. Therefore, a relatively strong temperature and salinity relaxation with an e-folding time of ~30 days is applied for the upper 200 m and a weaker relaxation below 200 m with an e-folding time of 5 years. This set of relaxation coefficients allows us to obtain the interdecadal GMOC changes that are consistent with the decadally averaged hydrographic observations while maintaining a realistic pattern of the GMOC.

Data-constrained diagnostic ocean & sea-ice model simulations. During the spin-up run, the surface flux fields in each model year were randomly selected from the period of 1955–1974, following the time-shuffling spin-up method used in Lee et al.[95]. After the spin-up, the CESM1 ocean & sea-ice model run was continued for 100 years using the surface flux fields in each model year randomly selected from

the period of 1955–1964, and its temperature and salinity fields relaxed to the decadally averaged WOA18 for the period of 1955–1964. The same model experiment was repeated for each of the other five decadal periods of 1965–1974, 1975–1984,1985–1994, 1995–2004, and 2005–2017. The spin-up run was also continued for an additional 100 years, which is used as the reference to describe the GMOC and its changes during each decade. The six model runs for different decadal periods and the reference run all used the same initial conditions derived from the spin-up run.

In addition to this primary set of data-constrained model simulations, we also carried out two sets of sensitivity experiments. In the first set, the model temperature and salinity fields were relaxed to the decadally averaged EN4 dataset[79] with temperature bias corrections to historical expendable bathythermograph observations[80] replacing the decadally averaged WOA18. In the second set, the surface forcing fields derived from the ERA5 were replaced by those derived from the Japanese 55-year reanalysis (JRA55)[82].

Data availability

The World Ocean Atlas 18 (WOA18) data were downloaded from NOAA's National Centers for Environmental Information at https://www.ncei.noaa.gov/access/world-ocean-atlas-2018. The EN4 temperature and salinity data were downloaded from the UK Met Office at https://www.metoffice.gov.uk/hadobs/en4. The European Center for Medium-Range Weather Forecasts (ECMWF) reanalysis-5 (ERA5) surface flux data were downloaded from ECMWF at https://www.ecmwf.int/en/forecasts/dataset/ecmwf-reanalysis-v5. The Japanese 55-year reanalysis (JRA55) surface flux data were downloaded from the National Center for Atmospheric Research at https://rda.ucar.edu/datasets/ds628.0. The monthly time series of the North Atlantic Oscillation (NAO) index were downloaded from NOAA's Climate Prediction Center (CPC) at https://www.cpc.ncep.noaa.gov/products/precip/CWlink/pna/nao.shtml. All other data used in this study are available from https://doi.org/10.25921/b70d-ck21.

Code availability

The code of the Community Earth System Model version 1 (CESM1) is publicly available from the National Center for Atmospheric Research at https://www.cesm.ucar.edu/models/cesm1.0.

Received: 22 July 2022; Accepted: 21 February 2023;
Published online: 13 March 2023

References

1. Li, G. et al. Increasing ocean stratification over the past half-century. *Nat. Clim. Change* **10**, 1116–1123 (2020).
2. Gordon, A. L. Interocean exchange of thermocline water. *J. Geophys. Res.: Oceans* **91**, 5037–5046 (1986).
3. Broecker, W. S. The biggest chill. *Nat. Hist. Mag.* **96**, 74–82 (1987).
4. Macdonald, A. M. & Wunsch, C. An estimate of global ocean circulation and heat fluxes. *Nature* **382**, 436–439 (1996).
5. Sarmiento, J. L. & Le Quere, C. Oceanic carbon dioxide uptake in a model of century-scale global warming. *Science* **274**, 1346–1350 (1996).
6. Talley, L. D. Shallow, intermediate, and deep overturning components of the global heat budget. *J. Phys. Oceanogr.* **33**, 530–560 (2003).
7. Talley, L. D. Freshwater transport estimates and the global overturning circulation: shallow, deep and throughflow components. *Prog. Oceanogr.* **78**, 257–303 (2008).
8. Evans, G. R. et al. South Atlantic interbasin exchanges of mass, heat, salt and anthropogenic carbon. *Prog. Oceanogr.* **151**, 62–82 (2017).
9. Zhang, R. et al. A review of the role of the Atlantic Meridional Overturning Circulation in Atlantic Multidecadal Variability and associated climate impacts. *Rev. Geophys.* **57**, 316–375 (2019).
10. Little, C. M. et al. The Relationship between U.S. East Coast sea level and the Atlantic Meridional Overturning Circulation: a review. *J. Geophys. Res. Oceans* **124**, 6435–6458 (2019).
11. Aoki, S., Rintoul, S. R., Ushio, S., Watanabe, S. & Bindoff, N. L. Freshening of the Adélie land bottom water near 140°E. *Geophys. Res. Lett.* **32**, L23601 (2005).
12. Rintoul, S. R. Rapid freshening of Antarctic Bottom Water formed in the Indian and Pacific Oceans. *Geophys. Res. Lett.* **34**, L06606 (2007).
13. Johnson, G. C., Purkey, S. G. & Bullister, J. L. Warming and freshening in the abyssal southeastern Indian Ocean. *J. Clim* **21**, 5351–5363 (2008).
14. Purkey, S. G. & Johnson, G. C. Warming of global abyssal and deep Southern Ocean waters between the 1990s and 2000s: contributions to global heat and sea level rise budgets. *J. Clim.* **23**, 6336–6351 (2010).
15. Purkey, S. G. & Johnson, G. C. Global contraction of Antarctic Bottom Water between the 1980s and 2000s. *J. Clim.* **25**, 5830–5844 (2012).
16. Purkey, S. G. & Johnson, G. C. Antarctic Bottom Water warming and freshening: contributions to sea level rise, ocean freshwater budgets, and global heat gain. *J. Clim.* **26**, 6105–6122 (2013).
17. Shimada, K., Aoki, S., Ohshima, K. I. & Rintoul, S. R. Influence of Ross Sea Bottom Water changes on the warming and freshening of the Antarctic Bottom Water in the Australian-Antarctic Basin. *Ocean Sci.* **8**, 419–432 (2012).
18. Aoki, S. et al. Widespread freshening in the Seasonal Ice Zone near 140°E off the Adélie Land Coast, Antarctica, from 1994 to 2012. *J. Geophys. Res. Oceans* **118**, 6046–6063 (2013).
19. Jullion, L. et al. Decadal freshening of the Antarctic Bottom Water exported from the Weddell Sea. *J. Clim.* **26**, 8111–8125 (2013).
20. van Wijk, E. M. & Rintoul, S. R. Freshening drives contraction of Antarctic Bottom Water in the Australian Antarctic Basin. *Geophys. Res. Lett.* **41**, 1657–1664 (2014).
21. Menezes, V. V., Macdonald, A. M. & Schatzman, C. Accelerated freshening of Antarctic Bottom Water over the last decade in the Southern Indian Ocean. *Sci. Adv.* **3**, e1601426 (2017).
22. Smeed, D. A. et al. The North Atlantic Ocean is in a state of reduced overturning. *Geophys. Res. Lett.* **45**, 1527–1533 (2018).
23. Silvano, A. et al. Recent recovery of Antarctic Bottom Water formation in the Ross Sea driven by climate anomalies. *Nat. Geosci.* **13**, 780–786 (2020).
24. Strass, V. H., Rohardt, G., Kanzow, T., Hoppema, M. & Boebel, O. Multidecadal warming and density loss in the deep Weddell Sea, Antarctica. *J. Clim.* **33**, 9863–9881 (2020).
25. Sen Gupta, A. et al. Projected changes to the Southern Hemisphere ocean and sea ice in the IPCC AR4 climate models. *J. Clim.* **22**, 3047–3078 (2009).
26. Weaver, A. J. et al. Stability of the Atlantic meridional overturning circulation: a model Intercomparison. *Geophys. Res. Lett.* **39**, L20709 (2012).
27. Cheng, W., Chiang, J. C. & Zhang, D. Atlantic meridional overturning circulation (AMOC) in CMIP5 models: RCP and historical simulations. *J. Clim.* **26**, 7187–7197 (2013).
28. Downes, S. M. & Hogg, A. M. Southern Ocean circulation and eddy compensation in CMIP5 models. *J. Clim* **26**, 7198–7220 (2013).
29. Sallée, J.-B. et al. Assessment of Southern Ocean water mass circulation and characteristics in CMIP5 models: historical bias and forcing response. *J. Geophys. Res. Oceans* **118**, 1830–1844 (2013).
30. Meijers, A. J. S. The Southern Ocean in the Coupled Model Intercomparison Project phase 5. *Philos. Trans. Royal Soc.* **372**, 20130296 (2014).
31. Weijer, W., Cheng, W., Garuba, O. A., Hu, A. & Nadiga, B. T. CMIP6 models predict significant 21st century decline of the Atlantic Meridional Overturning Circulation. *Geophys. Res. Lett.* **47**, e2019GL086075 (2020).
32. Gillett, N. P. & Thompson, D. W. J. Simulation of recent Southern Hemisphere climate change. *Science* **302**, 273–275 (2003).
33. Shindell, D. T. & Schmidt, G. A. Southern Hemisphere climate response to ozone changes and greenhouse gas increases. *Geophys. Res. Lett.* **31**, L18209 (2004).
34. Son, S.-W. et al. The impact of stratospheric ozone recovery on the Southern Hemisphere westerly jet. *Science* **320**, 1486–1489 (2008).
35. Lee, S. & Feldstein, S. B. Detecting ozone-and greenhouse gas-driven wind trends with observational data. *Science* **339**, 563–567 (2013).
36. Li, S., Liu, W., Lyu, K. & Zhang, X. The effects of historical ozone changes on Southern Ocean heat uptake and storage. *Clim. Dyn.* **57**, 2269–2285 (2021).
37. Waugh, D. W., Primeau, F., DeVries, T. & Holzer, M. Recent changes in the ventilation of the southern oceans. *Science* **339**, 568–570 (2013).
38. Gent, P. R. & Danabasoglu, G. Response to increasing Southern Hemisphere winds in CCSM4. *J. Clim.* **24**, 4992–4998 (2011).
39. Bishop, S. P. et al. Southern Ocean overturning compensation in an eddy-resolving climate simulation. *J. Phys. Oceanogr.* **46**, 1575–1592 (2016).
40. Gent, P. R. Effects of Southern Hemisphere wind changes on the meridional overturning circulation in ocean models. *Ann. Rev. Mar. Sci.* **8**, 79–94 (2016).
41. Marshall, J. & Radko, T. Residual-mean solutions for the Antarctic Circumpolar Current and its associated overturning circulation. *J. Phys. Oceanogr.* **33**, 2341–2354 (2003).
42. Farneti, R. et al. An assessment of Antarctic Circumpolar Current and Southern Ocean meridional overturning circulation during 1958–2007 in a suite of interannual CORE-II simulations. *Ocean Model.* **93**, 84–120 (2015).
43. Latif, M., Sun, J., Visbeck, M. & Bordbar, M. H. Natural variability has dominated Atlantic Meridional Overturning Circulation since 1900. *Nat. Clim. Change* **12**, 455–460 (2022).
44. Lee, S.-K. et al. Global meridional overturning circulation inferred from a data-constrained ocean & sea-ice model. *Geophys. Res. Lett.* **46**, 1521–1530 (2019).
45. Zhang, R. & Thomas, M. Horizontal circulation across density surfaces contributes substantially to the long-term mean northern Atlantic Meridional Overturning Circulation. *Commun. Earth Environ.* **2**, 112 (2021).
46. Sarmiento, J. L. & Bryan, K. An ocean transport model for the North Atlantic. *J. Geophys. Res. Oceans* **87**, 394–408 (1982).
47. Talley, L. D., Pickard, G. L., Emery, W. J. & Swift, J. H. *Descriptive Physical Oceanography: An Introduction* 6th edn 303–362 (Elsevier, 2011).

48. Talley, L. D. Closure of the global overturning circulation through the Indian, Pacific, and Southern Oceans: Schematics and transports. *Oceanogr.* **26**, 80–97 (2013).
49. McCartney, M. S. Subantarctic Mode Water. *Deep-Sea Res.* **24**, 103–119 (1977).
50. Sloyan, B. M. & Rintoul, S. R. Circulation, renewal, and modification of Antarctic Mode and Intermediate Water. *J. Phys. Oceanogr.* **31**, 1005–1030 (2001).
51. Eden, C. & Willebrand, J. Mechanism of interannual to decadal variability of the North Atlantic Circulation. *J. Clim.* **14**, 2266–2280 (2001).
52. Danabasoglu, G. et al. North Atlantic simulations in Coordinated Ocean-ice Reference Experiments phase II (CORE-II). Part II: Inter-annual to decadal variability. *Ocean Model.* **97**, 65–90 (2016).
53. Jackson, L. C. et al. The evolution of the North Atlantic Meridional Overturning Circulation since 1980. *Nat. Rev. Earth Environ.* **3**, 241–254 (2022).
54. Xu, X., Chassignet, E. P. & Wang, F. On the variability of the Atlantic meridional overturning circulation transports in coupled CMIP5 simulations. *Clim. Dyn.* **52**, 6511–6531 (2019).
55. Delworth, T. L. & Zeng, F. The impact of the North Atlantic Oscillation on climate through its influence on the Atlantic Meridional Overturning Circulation. *J. Clim.* **29**, 941–962 (2016).
56. Yashayaev, I. Hydrographic changes in the Labrador Sea, 1960−2005. *Prog. Oceanogr.* **73**, 242–276 (2007).
57. Jackson, L. C. et al. The mean state and variability of the North Atlantic circulation: a perspective from ocean reanalyses. *J. Geophys. Res. Oceans* **124**, 9141–9170 (2019).
58. Worthington, E. L. et al. A 30-year reconstruction of the Atlantic meridional overturning circulation shows no decline. *Ocean Sci.* **17**, 285–299 (2021).
59. Caínzos, V. et al. Thirty years of GOSHIP and WOCE data: Atlantic Overturning of mass, heat, and freshwater transport. *Geophys. Res. Lett.* **49**, e2021GL096527 (2022).
60. Caesar, L., Rahmstorf, S., Robinson, A., Feulner, G. & Saba, V. Observed fingerprint of a weakening Atlantic Ocean overturning circulation. *Nature* **556**, 191–196 (2018).
61. Rahmstorf, S. et al. Exceptional twentieth-century slowdown in Atlantic Ocean overturning circulation. *Nat. Clim. Change* **5**, 475–480 (2015).
62. Yang, Q. et al. Recent increases in Arctic freshwater flux affects Labrador Sea convection and Atlantic overturning circulation. *Nat. Commun.* **7**, 10525 (2016).
63. Moore, G. W. K., Våge, K., Pickart, R. S. & Renfrew, I. A. Decreasing intensity of open-ocean convection in the Greenland and Iceland seas. *Nat. Clim. Change* **5**, 877–882 (2015).
64. Moore, G. W. K., Våge, K., Renfrew, I. A. & Pickart, R. S. Sea-ice retreat suggests re-organization of water mass transformation in the Nordic and Barents Seas. *Nat. Commun.* **13**, 67 (2022).
65. Sévellec, F., Fedorov, A. & Liu, W. Arctic sea-ice decline weakens the Atlantic Meridional Overturning Circulation. *Nat. Clim. Change* **7**, 604–610 (2017).
66. Speer, K., Rintoul, S. R. & Sloyan, B. The diabatic Deacon Cell. *J. Phys. Oceanogr.* **30**, 3212–3222 (2000).
67. Döös, K. & Webb, D. J. The Deacon Cell and the other meridional cells of the Southern Ocean. *J. Phys. Oceanogr.* **24**, 429–442 (1994).
68. Polvani, L. M., Waugh, D. W., Correa, G. J. P. & Son, S. Stratospheric ozone depletion: the main driver of twentieth-century atmospheric circulation changes in the Southern Hemisphere. *J. Clim.* **24**, 795–812 (2011).
69. Kang, S. M., Polvani, L. M., Fyfe, J. C. & Sigmond, M. Impact of polar ozone depletion on subtropical precipitation. *Science* **332**, 951–954 (2011).
70. Lim, E.-P. et al. The impact of the Southern Annular Mode on future changes in Southern Hemisphere rainfall. *Geophys. Res. Lett.* **43**, 7160–7167 (2016).
71. Silvestri, G. E. & Vera, C. S. Antarctic Oscillation signal on precipitation anomalies over southeastern South America. *Geophys. Res. Lett.* **30**, 2115 (2003).
72. Hendon, H. H., Lim, E. & Nguyen, H. Seasonal variations of subtropical precipitation associated with the Southern Annular Mode. *J. Clim.* **27**, 3446–3460 (2014).
73. Farneti, R., Delworth, T. L., Rosati, A. J., Griffies, S. M. & Zeng, F. The Role of mesoscale eddies in the rectification of the Southern Ocean response to climate change. *J. Phys. Oceanogr.* **40**, 1539–1557 (2010).
74. Jacobs, S. S., Giulivi, C. F. & Mele, P. A. Freshening of the Ross Sea during the late 20th century. *Science* **297**, 386–389 (2002).
75. Jacobs, S. S. & Giulivi, C. F. Large multidecadal salinity trends near the Pacific–Antarctic continental margin. *J. Clim.* **23**, 4508–4524 (2010).
76. Williams, G. et al. The suppression of Antarctic bottom water formation by melting ice shelves in Prydz Bay. *Nat. Commun.* **7**, 12577 (2016).
77. Locarnini, R. A. et al. *World Ocean Atlas 2018, Volume 1: Temperature* (eds Mishonov, A.) Vol. 81, 52 (NOAA Atlas NESDIS, 2018).
78. Zweng, M. et al. *World Ocean Atlas 2018, Volume 2: Salinity* (eds Mishonov, A.) Vol. 82, 50 (NOAA Atlas NESDIS, 2018).
79. Good, S. A., Martin, M. J. & Rayner, N. A. EN4: Quality controlled ocean temperature and salinity profiles and monthly objective analyses with uncertainty estimates. *J. Geophys. Res. Oceans* **118**, 6704–6716 (2013).
80. Cheng, L., Zhu, J., Cowley, R., Boyer, T. & Wijffels, S. Time, probe type, and temperature variable bias corrections to historical expendable bathythermograph observations. *J. Atmos. Ocean. Technol.* **31**, 1793–1825 (2014).
81. Hersbach, H. et al. The ERA5 global reanalysis. *Q. J. R. Meteorol. Soc.* **146**, 1999–2049 (2020).
82. Onogi, K. et al. The JRA-25 reanalysis. *J. Meteorol. Soc. Japan* **85**, 369–432 (2007).
83. Bronselaer, B. & Zanna, L. Heat and carbon coupling reveals ocean warming due to circulation changes. *Nature* **584**, 227–233 (2020).
84. Armour, K., Marshall, J., Scott, J., Donohoe, A. & Newsom, E. R. Southern Ocean warming delayed by circumpolar upwelling and equatorward transport. *Nat. Geosci.* **9**, 549–554 (2016).
85. Durack, P. J. & Wijffels, S. E. Fifty-year trends in global ocean salinities and their relationship to broad-scale warming. *J. Clim.* **23**, 4342–4362 (2010).
86. Lumpkin, R. & Speer, K. Global ocean meridional overturning. *J. Phys. Oceanogr.* **37**, 2550–2562 (2007).
87. Johnson, G. C. Quantifying Antarctic Bottom Water and North Atlantic Deep Water volumes. *J. Geophys. Res.* **113**, C05027 (2008).
88. Danabasoglu, G. et al. The CCSM4 ocean component. *J. Clim.* **25**, 1361–1389 (2012).
89. Gent, P. R. & McWilliams, J. C. Isopycnal mixing in ocean circulation models. *J. Phys. Oceanogr.* **20**, 150–155 (1990).
90. Danabasoglu, G. & Marshall, J. Effects of vertical variations of thickness diffusivity in an ocean general circulation model. *Ocean Model.* **18**, 122–141 (2007).
91. Jansen, M. F., Nadeau, L.-P. & Merlis, T. M. Transient versus equilibrium response of the ocean's overturning circulation to warming. *J. Clim.* **31**, 5147–5163 (2018).
92. Sun, S., Thompson, A. F. & Eisenman, I. Transient overturning compensation between Atlantic and Indo-Pacific basins. *J. Phys. Oceanogr.* **50**, 2151–2172 (2022).
93. Thompson, A. F., Hines, S. K. & Adkins, J. F. A Southern Ocean mechanism for the interhemispheric coupling and phasing of the bipolar seesaw. *J. Clim.* **32**, 4347–4365 (2019).
94. Webb, D., Spence, P., Holmes, R. & England, M. Planetary-wave-induced strengthening of the AMOC forced by poleward intensified southern hemisphere westerly winds. *J. Clim.* **34**, 7073–7090 (2021).
95. Lee, S.-K. et al. Wind-driven ocean dynamics impact on the contrasting sea-ice trends around West Antarctica. *J. Geophys. Res. Oceans* **122**, 4413–4430 (2017).

Acknowledgements

The authors acknowledge Denis Volkov for helpful discussions and comments, and Franz Philip Tuchen for reviewing the manuscript. This work was supported by the base funding of NOAA's Atlantic Oceanographic and Meteorological Laboratory (AOML), and by NOAA's Climate Program Office's Modeling, Analysis, Predictions, and Projections program. S.Y. acknowledges support from the Regional and Global Model Analysis (RGMA) component of the Earth and Environmental System Modeling Program of the U.S. Department of Energy's Office of Biological & Environmental Research (BER) under Award Number DE-SC0022070, and from the National Center for Atmospheric Research, which is a major facility sponsored by the National Science Foundation (NSF) under Cooperative Agreement No. 1852977. F.T., W.A., and D.K. were supported by NOAA's AOML in part under the auspices of the Cooperative Institute for Marine and Atmospheric Studies (CIMAS), a cooperative institute of the University of Miami and NOAA, cooperative agreement NA20OAR4320472.

Author contributions

S.-K.L. conceived the study, performed the analysis and wrote the initial draft of the paper. S.-K.L. carried out the data-constrained diagnostic ocean & sea-ice model simulations. F.G. and D.K. assisted the model simulations. All authors (S.-K.L., R.L., F.G., S.Y., H.L., F.T., S.D, W.A., D.K., and M.B.) significantly contributed to the discussion and interpretation of results, and reviewed and edited the paper.

Competing interests

The authors declare no competing interests.

Additional information

Supplementary information The online version contains supplementary material available at https://doi.org/10.1038/s43247-023-00727-3.

Correspondence and requests for materials should be addressed to Sang-Ki Lee.

Peer review information *Communications Earth & Environment* thanks Jia-Rui Shi and the other, anonymous, reviewer(s) for their contribution to the peer review of this work. Primary Handling Editors: Viviane V. Menezes and Clare Davis. Peer reviewer reports are available.